



Low dimensional Bi₂Se₃ NPs/reduced graphene oxide nanocomposite for simultaneous detection of L-Dopa and acetaminophen in presence of ascorbic acid in biological samples and pharmaceuticals

Govinda Gorle¹ · Ayyappa Bathinapatla^{1,2} · Suvardhan Kanchi^{3,4} · Yong Chien Ling¹ · Mashallah Rezakazemi⁵ 

Received: 19 March 2021 / Accepted: 10 July 2021 / Published online: 20 July 2021
© Islamic Azad University 2021

Abstract

Graphene-based inorganic layered materials have developed as a versatile, new class of nanomaterials and drawn huge scientific interest, owing to its thickness-dependent physical properties, exfoliated two-dimensional crystals in various technological and industrial applications. This work is the first demonstration of the fabrication of low dimensional bismuth selenide (Bi₂Se₃) NPs functionalized reduced graphene oxide (rGO) on the platinum electrode (Pt-E) for the ultra-sensitive and simultaneous detection of acetaminophen (ACT) and L-DOPA (LD) in the presence of ascorbic acid (AA) in various biological samples and pharmaceuticals. The constructed electrode accelerates the electron transfer reactions of LD and ACT without interfering with the electron transfer reactions of AA, which was an electroactive coexisting chemical. At pH 6.0 in 0.1 M phosphate buffer solution, Bi₂Se₃ NPs/rGO/Pt-E showed a sixfold and fivefold increase in cyclic voltammetry for LD and ACT signals, respectively, when compared to bare Pt-E. Under the optimal conditions, differential pulse voltammetry (DPV) demonstrated that the anodic peak currents were linearly dependent on the concentrations of LD (0.006–0.25 mM) and ACT (0.0045–0.14 mM) at anodic peak potentials of +0.25 and +0.52 V, respectively. With a signal to noise (S/N) ratio of 3, acceptable detection limits of 0.23 and 0.17 M were achieved for both LD and ACT, with strong intra- and inter-electrode repeatability. Overall, the fabricated nanosensor offered numerous advantages including ease to fabricate, ultra-sensitivity, good stability, and reproducibility towards the detection of LD and ACT in various biological samples and pharmaceuticals. The amounts of LD and ACT were also identified in commercial pharmaceuticals and synthetic urine samples to validate the applicability of the modified electrode.

Keywords Acetaminophen · Ascorbic acid · Bi₂Se₃ NPs · Graphene oxide · Nanosensor · Biological samples · Pharmaceuticals

✉ Suvardhan Kanchi
ksuvardhan@gmail.com

✉ Mashallah Rezakazemi
mashallah.rezakazemi@gmail.com

Yong Chien Ling
ycling@mx.nthu.edu.tw

¹ Department of Chemistry, National Tsing Hua University, Hsinchu 30013, Taiwan, ROC

² Department of Chemistry, Raghu Engineering College (Autonomous), Dakamarri (v), Bheemunipatnam, Visakhapatnam 531162, Andhra Pradesh, India

³ Department of Chemistry, Durban University of Technology, Durban 4000, South Africa

⁴ Department of Chemistry, Sambhram Institute of Technology, M.S. Palya, Jalahalli East, Bengaluru 560097, India

⁵ Faculty of Chemical and Materials Engineering, Shahrood University of Technology, Shahrood, Iran



Introduction

Parkinson's disease (PD) is one of the life-threatening diseases caused by an imbalance production of dopamine in the brain [1]. This can be prevented by increasing the dopamine levels with various drugs such as Levodopa (L-3,4-dihydroxyphenylalanine, LD). In humans, the LD can be biosynthetically prepared from non-essential amino acid such as tyrosine. However, the LD can autoxidize in the peripheral system and leads to various side effects, for instance, dyskinesia, vomiting, nausea, paranoia, and schizophrenia [2]. Therefore, it is essential to control its dosage by detecting the amount of LD. Keeping in mind, different analytical approaches have been proposed, including high-performance liquid chromatography [3], spectroscopy [4], flow injection analysis [5], gas chromatography [6], and capillary electrophoresis [7] for the determination of LD in pharmaceutical and biological samples.

Moreover, Acetaminophen (ACT) or Paracetamol is one of the most extensively used drugs for reducing fevers originated from bacteria or viruses, and pain caused by arthritis, backaches, headaches, and post-operation aches. Further, the patients those sensitive to aspirin can use ACT as an effective substitute and it is safe up to therapeutic doses. The ACT has an admirable safety profile due to its highest (90%) absorption capacity by the organism and then excreted through urine. However, higher doses of AC can cause nephrotoxicity and severe or sometimes fatal hepatotoxicity. Therefore, to determine ACT levels, several analytical procedures have been developed in the literature such as near-infrared transmittance spectroscopy [8], spectrofluorimetry [9], and high-performance liquid chromatography [10], spectrophotometry [11], capillary electrophoresis [12]. However, these methods are still limited due to their process complexity, non-economic, prolonged time for analysis. Whereas electrochemical techniques have superior advantages such as cost-effectiveness, sensitivity, rapidness, simplicity, and user friendly. Moreover, it is renowned that chemically modified electrodes are widely used in various fields such as clinical, environmental applications as a selective and sensitive analytical tool. Recently, researchers are focused on the design and development of sensors using the electrodes modified with nanocomposites, results in the amplification of electroanalytical signals [13]. By utilizing these features, electrodes modified with various functional materials including Au–Pd/NPSS [14], 4-MoPD/MWCNTs [15], g-C₃N₄-E-PEDOT [16] and Poly (L-Dopa)/MWCNTs [17] has been used for the detection of ACT and LD.

Opiates were used by Parkinson's disease patients, drugs, and acetaminophen treating neuropathic pain such

as antiepileptics and antidepressants. The pharmacokinetics of ACT will greatly change by altering the gastric emptying with other drugs. In the human body, the absorption of ACT is exponentially dependent on gastric emptying [18]. Mostly, ascorbic acid (AA) is used as dietary food or medicine. Therefore, it is a great challenge to develop an analytical method to quantify drugs without the interference of AA for better health. The literature survey reveals that very few reports existed in the literature for the electrochemical detection of LD and ACT [18]. However, these methods have certain drawbacks such as low sensitivity and AA interference.

The sheets of graphene oxide (GO) are honeycomb-shaped crystal structures made up of monolayers of carbon atoms, have recently attracted a lot of attention because of their large surface-to-volume ratio, superior chemical stability, tuneable bandgap, and good thermal, mechanical, and electronic stabilities. [19]. The unique properties of the GO nanosheets motivated to utilize in various applications such as drug delivery, protein assays, biosensors and molecular probing of living cells [20].

Moreover, various nanostructures modified with GO such as MnO₂, ZnO, CuO, and Cr₃O₄, etc., have been recognized as promising electron mediators for the fabrication of sensitive electrochemical sensors [21]. Whereas packed advantages of bismuth have been already explored as a successful alternative electrode to substitute the noxious mercury electrode in anodic or cathodic stripping voltammetry [22]. In addition, various bismuth precursor materials were used as an electrochemical sensor, such as Bi₂O₃ [23], bismuth citrate [24], ammonium tetrafluorobismuthate [25], bismuth xerogel [26], bismuth phosphate [27]. It was demonstrated that the concentration of the bismuth precursors is greatly influenced the detection capabilities. Bismuth-related compounds were greatly utilized in electro-analysis of pharmaceuticals [28], hormones [29] pesticides [30], etc. As a result, innovative bismuth precursors are urgently needed in a variety of applications, including food [28], environmental [28], and clinical analysis [31]. Bismuth-based nanomaterials, on the other hand, have significant benefits over bulk bismuth precursors due to their increased surface area, chemical, and physical properties. Recently, Bismuth chalcogenides such as Bi₂Te₃, Bi₂S₃, and Bi₂Se₃ have gained much interest due to their 2D structures and superior performance for various applications [32]. The remarkable band gap approximately up to 0.3 eV of Bi₂Se₃ and its laminated structure with stacky layers (Se-Bi-Se-Bi-Se) makes it as a weak van der Waals interactions with the thickness of each layer of about 0.96 nm [32]. Overall, overcoming the limitations of the literature and leveraging the unique features of rGO and Bi to make the suggested electrochemical sensor highly selective for concomitant sensing of LD and ACT in the sight of AA is a difficult challenge.

In the present study, the Bi_2Se_3 NPs/rGO/Pt-E was successfully fabricated for concomitant determination of LD and ACT in the presence of AA. The present electrode system successfully overcomes the overlapping of oxidation peaks, resulted in the selective detection of targeted drugs compare to that of the unmodified electrode. Furthermore, reproducibility, ultra-sensitivity, stability, short-time response, vast linear range, and low detection limits made the Bi_2Se_3 NPs/rGO/Pt-E as a superior sensor.

Experimental

Chemicals and reagents

Levodopa (LD), Acetaminophen (ACT), Ascorbic acid (AA) standards of 97% analytical quality were obtained from Sigma Aldrich, Taiwan. For real sample analysis, LD and ACT pharmaceutical samples were obtained from a local pharmacy. Analytical grade bismuth (III) nitrate pentahydrate ($\text{Bi}(\text{NO}_3)_3 \cdot 0.5\text{H}_2\text{O}$) (98%), sodium selenite pentahydrate ($\text{Na}_2\text{SeO}_3 \cdot 0.5\text{H}_2\text{O}$) (99%), ethylene glycol, isopropyl alcohol, ethanol, nafion, were purchased from Sigma-Aldrich. Analytical grade disodium hydrogen orthophosphate and sodium dihydrogen orthophosphate, hydrochloric acid, sodium hydroxide, sulphuric acid were (Sigma Aldrich product) supplied by Uni-Onward Corporation (Taipei, Taiwan). Metrohm (Taipei, Taiwan) provided alumina powder with a particle size of 3 μm . Chiahlung (Taiwan) provided 99.9% of the nitrogen gas needed. Merck Millipore series water filtration provided deionized water for all solutions and samples (Merck SUPPORT, United States). For stability, all normal solutions were held at 4 °C in the Samsung refrigerator.

Instrumentation

All electrochemical measurements were carried out using Autolab/PGSTAT 204 connected to 663 VA stand and IME663 interface from Metrohm (Herisau, Switzerland) operated with a PC installed using NOVA 1.11 software. The three-electrode system consisting of the platinum electrode (Pt-E) with 3 mm diameter (working electrode), the platinum wire as a counter electrode, and Ag/AgCl as a reference electrode were used to record voltammograms at room temperature. Prior to analysis, all solutions were purged with pure (99.99%) nitrogen gas for 10 min. The pH measurements (CRISON micro pH 2000 digital pH meter) were recorded on a which was previously calibrated with a precision of 0.1 pH units using buffers of known pH. The as-prepared Bi_2Se_3 NPs and Bi_2Se_3 NPs/rGO were well characterized as follows. Powder X-ray diffraction (XRD) using a Rigaku D/MAX-2500 X-ray diffractometer with Cu $\text{K}\alpha$ radiation ($\lambda = 1.5406$

Å) at 40 kV and 20 mA was used to examine the crystal structures of the samples. The UV–Vis–NIR spectra for rGO, Bi_2Se_3 NPs, and Bi_2Se_3 NPs/GO were recorded using a JASCO V-570 spectrometer in the wavelength range of 350–1200 nm, with a resolution of 1 nm. The morphologies and elemental composition of the Bi_2Se_3 NPs and Bi_2Se_3 NPs/rGO were analyzed by a JEOL JEM-2100 TEM coupled with an EDXA analyzer as well as a JEOL, JSM-7000F SEM. A VG-ESCALAB 220 i-XL system was used for the XPS experiments. Bi_2Se_3 NPs/rGO samples were mounted on a sample holder and cleaned and measured in the same manner. The imaging capabilities of the system were used to regulate the probe zone on the surface. The chamber's base pressure was around 6×10^{-8} Pa, and the sample was not contaminated during the measurements.

Synthesis of rGO, Bi_2Se_3 NPs and Bi_2Se_3 NPs/rGO nanocomposite

Reduced graphene oxide was synthesized using the pristine graphite flakes as a starting material following by the modified Hummers process [33]. The Bi_2Se_3 NPs was synthesized by the reported procedure [34] with some modifications: 1 mM of $\text{Bi}(\text{NO}_3)_3$ and 1.5 mM of Na_2SeO_3 were stirred for 1 h in 35 mL of ethylene glycol after dissolving, the reaction mixture temperature was raised to 260 °C for 5 h and then cool down to room temperature. Isopropyl alcohol was added to the reaction mixture to precipitate the Bi_2Se_3 NPs, followed by acetone washings to remove unreacted components, ethylene glycol, and oven drying for 6 h at 50 °C.

Preparation of Bi_2Se_3 NPs/rGO nanocomposite

Bi_2Se_3 NPs/rGO hybrid dispersion was prepared as follows: Typically, Bi_2Se_3 NPs (0.5 mg mL^{-1}) and 0.5 mg mL^{-1} of rGO were added in 1 mL of ethanol: water (2:3) mixture. Finally, to the mixture, 100 μL of Nafion was added and sonicated for 1 h in an Elmasonic S40, 140 W sonication bath. Nafion acts as a binder to the electrode surface. Before modification of Pt-E, Bi_2Se_3 NPs/rGO nanocomposite was agitated for 4 h.

Preparation of working electrodes

A bare Pt-E was manually polished to a mirror-like surface with 3 μm alumina slurry followed by the rinsing with deionized distilled water. Thenafter, 3–5 drops of concentrated nitric acid in a deionized distilled water was added to perform the electrochemical cleaning at a potential range of -0.4 – 1.0 V for 30 cycles to remove physisorbed or chemisorbed materials from the surface of the electrode. After that, the Pt-E was coated with 6 μL of Bi_2Se_3 /rGO by gently dropping it onto the surface of the electrode and widely



distributed with a tip followed by the drying in a 50 °C oven for 10 min to obtain a Bi₂Se₃/rGO/Pt-E.

Preparation of stock solutions

In a 5.0 mL volumetric flask, standard solutions of AA, LD and ACT were prepared using appropriate quantities and further diluted with deionized distilled water. Similarly, 100 mL of 0.1 M phosphate buffer was prepared using dihydrogen orthophosphate and disodium hydrogen orthophosphate in deionised distilled water. The optimum pH of the solution was set to 6.0 by adding the appropriate amount of NaOH/HCl and stored at 4 °C. These solutions were cleaned before voltammetric measurements with a disposal syringe having a 25 mm diameter, 0.45 mm pore size cellulose filter.

Preparation of ACT and LD pharmaceuticals and synthetic urine samples

The ACT pharmaceuticals were prepared by crushing the three Ancogen tablets (250 mg mL⁻¹, Hua Shin Chemical Pharmaceutical works CO., LT, Taiwan) and three SOMA tablets (250 mg mL⁻¹, Standard Chem & Pharm CO., LTD, Taiwan) to a fine powder. An equivalent one tablet weight of the powder was dissolved in 25 mL of 0.1 M PBS at pH 6.0, ultrasonicated for 5 min, and diluted to 100 mL with PBS. The quantification of ACT and LD were performed with DPV using a regression equation. Similarly, LD in 1 mL of dopamine injection (40 mg mL⁻¹, Taiwan Biotech CO., LTD) was prepared by diluting 50 mL of 0.1 M PBS at pH 6.0.

The synthetic urine sample was prepared according to the literature [35]. 0.40 g KCl, 0.28 g CaCl₂·2H₂O, 0.73 g NaCl, 0.35 g KH₂PO₄, 0.56 g Na₂SO₄, 25 g NH₄Cl, and 6.25 g urea have been introduced to a 250 mL of volumetric flask with deionized distilled water. As synthetic urine samples were doped with three different concentrations of LD: 10, 15, and 25 μM and ACT: 10, 20, and 30 μM, respectively, and aliquots of each sample were diluted with supporting electrolyte solution and the final solutions were analyzed.

Procedure for the electrochemical measurement of LD and ACT

A 10 mL of 0.1 M PBS was added to an electrochemical cell equipped with bare Pt-E or Bi₂Se₃ NPs/rGO/Pt-E as a working electrode. After achieving low background current by several cyclic sweeps, an aliquot (analyte solution) was added and a pre-concentrated potential was applied with a stirring (400 rpm) of solution. The stirring was stopped at the end of the pre-concentration time and allowed for 5 s equilibration period to become inert. The DPV was recorded using the bare or Bi₂Se₃ NPs/rGO/Pt-E by positive scanning

mode at a rate of 0.1 V/s, for each measurement, the working electrode was cleaned with deionized distilled water.

Results and discussion

Characterization of Bi₂Se₃ NPs/rGO nanocomposite

Bi₂Se₃ NPs were synthesized by high-temperature reaction and further fabricated on graphene oxide through sonication process and characterized using different spectroscopic techniques. With scanning electron microscopy (SEM) and transmission electron microscopy (TEM), the morphologies and nanostructures of as-prepared Bi₂Se₃ NPs and Bi₂Se₃ NPs/rGO were investigated. The layer structure of Bi₂Se₃ NPs is depicted in SEM pictures (Fig. 1A, B), with some showing truncated trigonal morphology with an average size of 0.8–0.9 μm. Some are generated in the intermediate stage and show truncated trigonal morphology with an average size of 0.8–0.9 μm. Furthermore, as shown in Fig. 1B, the Bi₂Se₃ NPs were well penetrated by thin layers of rGO. In the image, the curves and outlines of overlap between two nanoplates could be seen. Low magnification bright-field TEM was used to corroborate the hexagonal morphology of the Bi₂Se₃ NPs, as shown in Fig. 1C.

The selected area electron diffraction (SAED) pattern (Fig. 1D) has a sixfold symmetry with a [0 0 1] zone axis pattern, which matches the prior study [36]. Figure 1E, F depict a thin layer of rGO nanosheets and hexagonal Bi₂Se₃ NPs wrapped in rGO layers, respectively. The chemical composition of Bi₂Se₃ NPs was determined by energy dispersive X-ray analysis (EDXA). The strong characteristic signals of Bi₂Se₃ NPs for Bi and Se at 1.9 keV, 2.52 keV and 1.47 keV respectively, as shown in Fig. 2A. The obtained results were in comparison with the literature [37, 38]. However, the weak signals of carbon, oxygen and copper at 0.25, 0.5, 1.0, 5.3 and 8 keV were observed due to the usage of copper grid during the analysis of transmission electron microscope. In the case of synthesis of AgNPs and AuNPs by the Singh and co-workers, similar minor peaks were also observed in the spectra of EDXA [39].

Furthermore, the synthesized Bi₂Se₃ NPs was also characterized by elemental mapping, in which the weight percentage (wt %) and of bismuth (Bi M) and selenium (Se L) were found to be 62.34% and 37.66% and atomic percentage (at %) of Bi M and Se L were 38.47% and 61.53%, respectively, as shown in Table 1. These results demonstrated that the at % of Bi M to Se L was found to be approximately 2:3, confirming the product to be Bi₂Se₃ [38].

The powder XRD patterns of the Bi₂Se₃ NPs, rGO, and Bi₂Se₃ NPs/rGO samples also confirmed phase composition and structural characteristics, as shown in Fig. 2B–D. Figure 2B shows the observed typical diffraction peaks

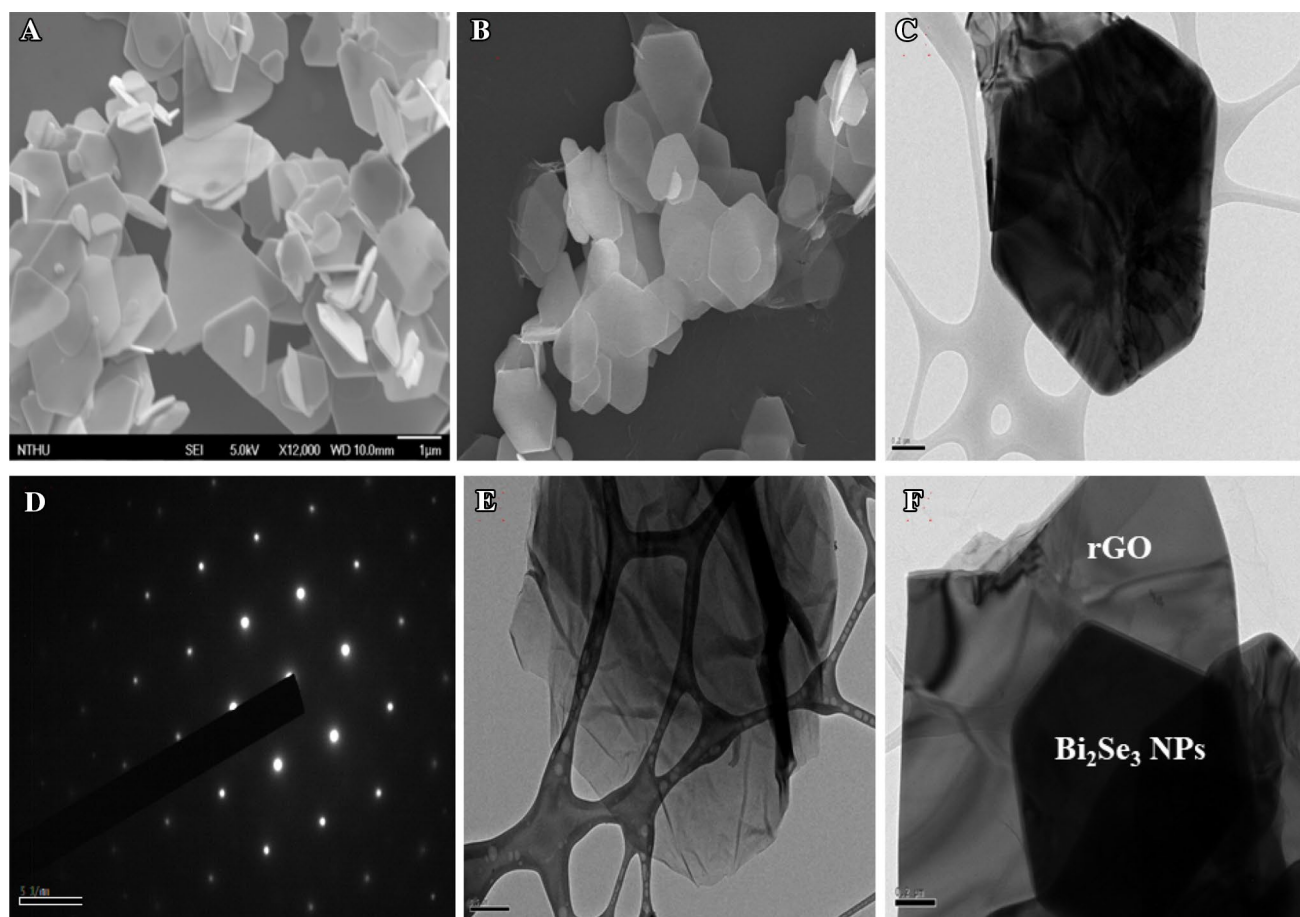


Fig. 1 SEM images of **A** Pure Bi_2Se_3 NPs **B** Bi_2Se_3 NPs/rGO, TEM images of **C** Pure Bi_2Se_3 NPs **D** Bright field emission spectra of Bi_2Se_3 NPs **E** TEM images of rGO **F** TEM images of Bi_2Se_3 NPs/rGO

of carbon in rGO (001) at $2\theta = 10^\circ$. XRD pattern for the orthorhombic structure of Bi_2Se_3 was illustrated in Fig. 2C. The obtained XRD diffraction peaks are consistent with the reported values (JCPDS Card No.33-0214) as per literature [40–42]. According to the previous study, (0 1 5), (1 0 1 0), (1 1 0) facets are the three strongest diffraction peaks at $2\theta = 41.3^\circ, 44.5^\circ, 48.7^\circ$ for Bi_2Se_3 NPs with reference to our previously reported paper [34]. Whereas a typical diffraction peak of rGO at $2\theta = 18.4^\circ$ has been noted in the XRD pattern of Bi_2Se_3 NPs/rGO nanocomposite as illustrated in Fig. 2D.

This indicates the proper matching of lattices between the counterparts which is favorable for the stability of nanocomposite. The UV–visible absorption spectrum of suspended rGO nanosheets is shown in Fig. 2E. The major absorption peak at about 230 nm is due to the $\pi \rightarrow \pi^*$ transitions of aromatic C–C bond, and a shoulder at about 300 nm can be assigned to the $\pi \rightarrow \pi^*$ transitions of C=O bonds which confirms the existence of oxygen functional groups in rGO nanosheets [43].

UV–vis–NIR spectra of graphene oxide have strongly dropped NIR absorbance however, Bi_2Se_3 NPs and Bi_2Se_3

NPs/rGO having broad NIR absorbance due to the strong absorption of light. XPS was used to investigate the surface chemical composition of Bi_2Se_3 NPs/rGO nanocomposite. The high-resolution spectra were recorded at a narrow energy range as shown in Fig. 2F. The major elements present in the composite Bi, Se, C, and O were determined at 157.8–163 eV, 53.7–54.3 eV, 284–289 eV, and 532 eV, respectively.

Figure 3A, B shows the C1s and O1s XPS spectra of rGO, respectively. The C–C and C–H binding energies were assigned at 284.5–285 eV, and chemical shifts of C–OH, C=O, and O=C–OH functional groups are +1.5, +2.5 and +3.7 eV, respectively [44]. The high-intensity peak at 532 eV represents the presence of a high amount of oxygen in the form of carboxylic, alcoholic groups in the composite (Fig. 3A). The high-resolution spectra of Bi4f (Fig. 3C) and Se3d (Fig. 3D) indicating that Bi4f peak exhibited much higher intensity than that of Se3d peak. Furthermore, Bi4f spectra revealed peaks at 158.2 and 163.8 eV for $\text{Bi}4f_{7/2}$ and $\text{Bi}4f_{5/2}$, respectively, which are consistent with literature [45]. Whereas, Se3d spectra showed a peak at 53.7 eV which



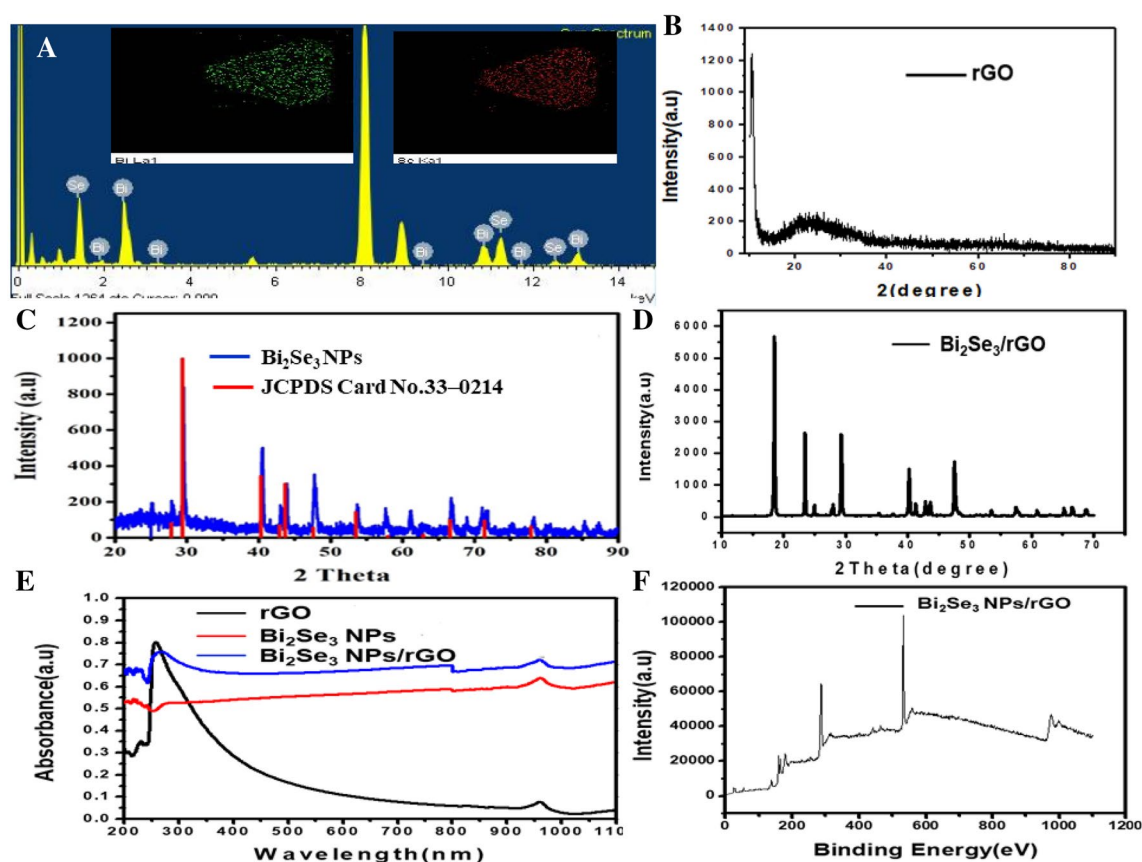


Fig. 2 A EDAX of pure Bi_2Se_3 NPs and in inset showing the Elemental mapping of Bi and Se B XRD for rGO C XRD for Bi_2Se_3 NPs D XRD for Bi_2Se_3 NPs/rGO E UV–Vis–NIR spectra for Bi_2Se_3 NPs, rGO and Bi_2Se_3 NPs/rGO F XPS spectra for Bi_2Se_3 NPs/rGO

Table 1 Analysis of elemental composition of Bi_2Se_3 NPs by EDXA

Element	Weight %	Atomic %	Total
Bi M	62.34	38.47	100.00
Se L	37.66	61.53	100.00

corresponds to the bonding energy of the Se3d transition. According to the peak areas of Bi4f and Se3d, the atomic ratio of Bi/Se was 40.5:59.5, indicating that Bi_2Se_3 NPs were formed with a high density of selenium vacancies.

The atomic force microscopy (AFM) analyses were performed to evaluate the surface morphology of the synthesized Bi_2Se_3 NPs/rGO nanocomposite. The AFM amplitude images in Fig. 4 demonstrates a hexagonal nanoplate with rGO sheets. The height profile indicates that the thickness increased from the edge to the center and the nanocomposite was in the size of 41 nm.

Optimization of solution pH and accumulation time

The electrochemical reaction of the developed Pt-E to LD and ACT was investigated in various electrolyte solutions,

including acetate buffer solution, Britton–Robinson buffer solution, and PBS at pH 6.0. The electrode had the highest sensitivity to LD and ACT of all the PBS solutions tested. The impact of pH on anodic peak potentials and anodic peak currents was also investigated. The DPV analyses were conducted for individual solutions of LD and ACT in the pH range of 4.0–8.0. As shown in Fig. 5A, B, the anodic peak currents (I_{pa}) varied with pH. Both LD and ACT oxidation peak currents increased when the pH climbed from 4.0 to 6.0. However, as the pH rises, the peak current decreases, indicating sluggish electron transfer kinetics. PBS with a pH of 6.0 was utilized as a supporting electrolyte for the simultaneous electrochemical detection of LD and ACT in the mixture based on the results.

Furthermore, the DPV analyses revealed that the peak potentials varied linearly with pH (Fig. 5A, B), as stated in the equations below:

$$E_{pa}(V) = 0.62 - 0.062\text{pH} \quad (R^2 = 0.999) \text{ LD} \quad (1)$$

$$E_{pa}(V) = 0.884 - 0.057\text{pH} \quad (R^2 = 0.9942) \text{ ACT} \quad (2)$$

The findings showed that as pH increased, the oxidation peak potentials of LD and ACT changed towards lower

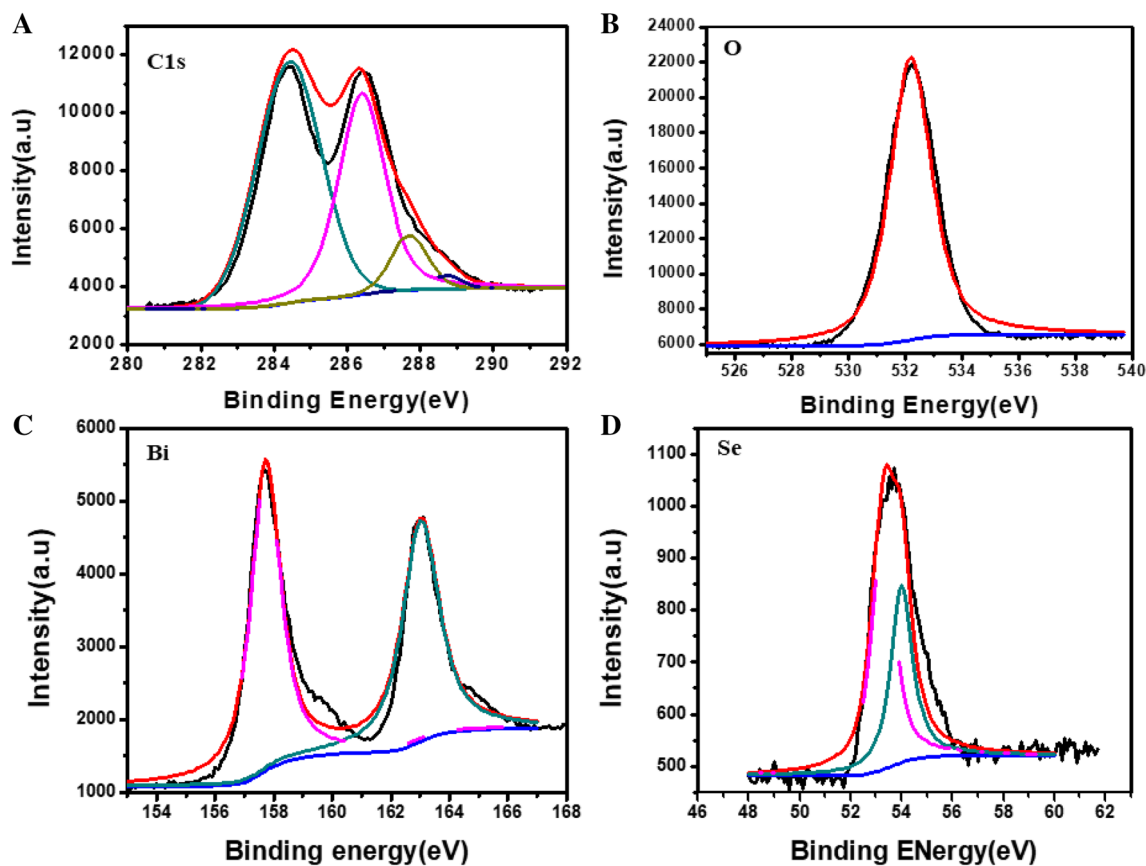


Fig. 3 XPS analysis for Bi_2Se_3 NPs/rGO composite A O1s B C1s C Bi D Se

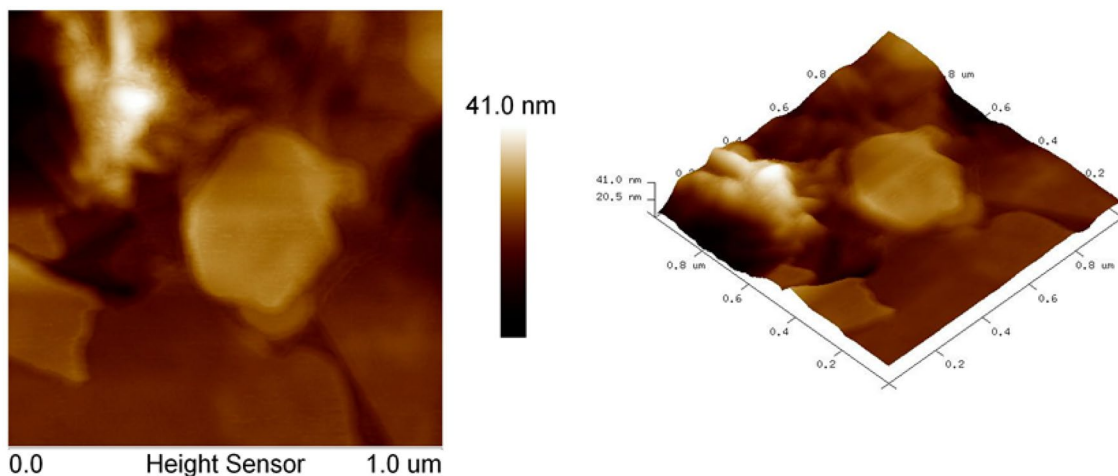


Fig. 4 Atomic force microscopy (AFM) analyses of the synthesized Bi_2Se_3 NPs/rGO nanocomposite

potentials, indicating that protons were transferred throughout the electrochemical process of LD and ACT. The slopes of oxidation peak potential (E_p) vs. pH at 25 °C were 62 mV/pH and 57 mV/pH for LD and ACT, respectively. These results demonstrated that the oxidation process of LD

and ACT at Bi_2Se_3 NPs/rGO/Pt-E required a same number of protons and electrons, which was calculated as 2. Figure 5C, D represents the cyclic voltammograms of 0.5 mM LD and ACT recorded at Pt-E modified with rGO, Bi_2Se_3 NPs and Bi_2Se_3 NPs/rGO. The results clearly demonstrated

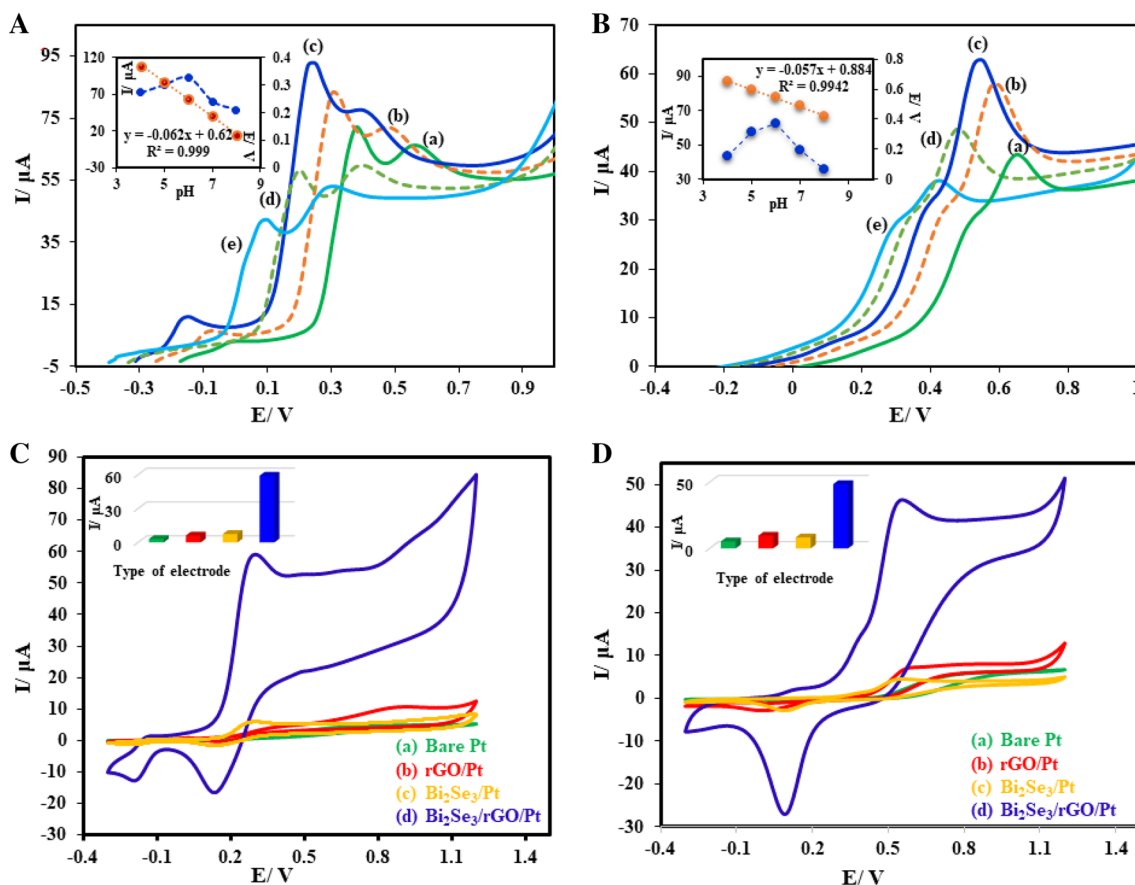


Fig. 5 Cyclic voltammograms recorded at different pHs (4.0–8.0) with 0.5 mM concentration of **A** LD **B** ACT (in inset) shows the effect of pH on peak potentials and current. Cyclic voltammograms of

0.5 mM **C** LD and **D** ACT at **a** bare Pt-E **b** rGO/Pt-E **c** Bi₂Se₃ NPs/rGO/Pt-E, inset: current comparison among three electrodes in both cases

that the electrochemical signals obtained with Bi₂Se₃ NPs/rGO were much higher than that of rGO and Bi₂Se₃ NPs in both cases.

Figure 6 represents the electrode mechanism of LD and ACT at Bi₂Se₃ NPs/rGO/Pt-E. The sensitivity of the electrode towards analytes can be enhanced by accumulation studies that are simple and effective. Accumulation time and potential studies were carried out with 0.5 mM ACT and LD at Bi₂Se₃ NPs/rGO/Pt-E. Figure 7A depicts the effect of accumulation potential on ACT and LD oxidation peak currents. In the potential range of -0.6 – 0.8 V, the variation in the anodic peak currents of LD and ACT with the accumulating potential was investigated. As shown in Fig. 7B, the anodic peak currents increased as accumulation potential decreased from 0.8 to -0.5 V. However, the peak current was unchanged with higher negative potentials. Therefore, -0.2 V was chosen as accumulation potential for further studies. The influence of the accumulation period on the anodic peak currents of LD and ACT was investigated at a fixed accumulation potential of -0.2 V, as shown in Fig. 7B. For achieving fair detection limits in voltammetry,

accumulation time is an important factor. As the accumulation time increases from 10 to 150 s, the peak current also increased. The extended accumulation time would give a better platform for the LD and ACT to complete their oxidation reactions, leading in a greater peak current. However, when the accumulation time rose, the peak current remained unchanged due to the oxidized LD and ACT reaching saturation of modified Pt-E. As a result, a 100 s accumulation time was chosen for further research.

Electrochemical characterization of Bi₂Se₃ NPs/rGO/Pt-E

The microscopic areas of the Bi₂Se₃ NPs/rGO/Pt-E were electrochemically measured using 1 M K₃Fe(CN)₆ as a probe solution with cyclic voltammetry (CV). One-electron transfer reaction ($n=1$) was seen in the [Fe(CN)₆]³⁻, which is one of the most investigated redox coupling reactions in the field of electrochemistry. The cathodic and anodic peak currents of the redox probe increase linearly with the increase in the scan rate increase from 10 to 210 mV/s.

Fig. 6 Fabrication of Pt-E with Bi_2Se_3 NPs/rGO nanocomposite and electrochemical mechanism for LD, ACT in the presence of AA

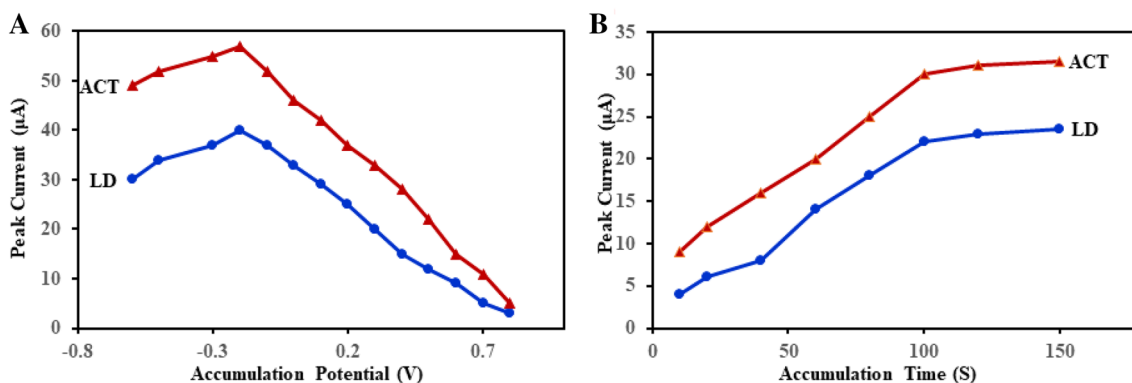
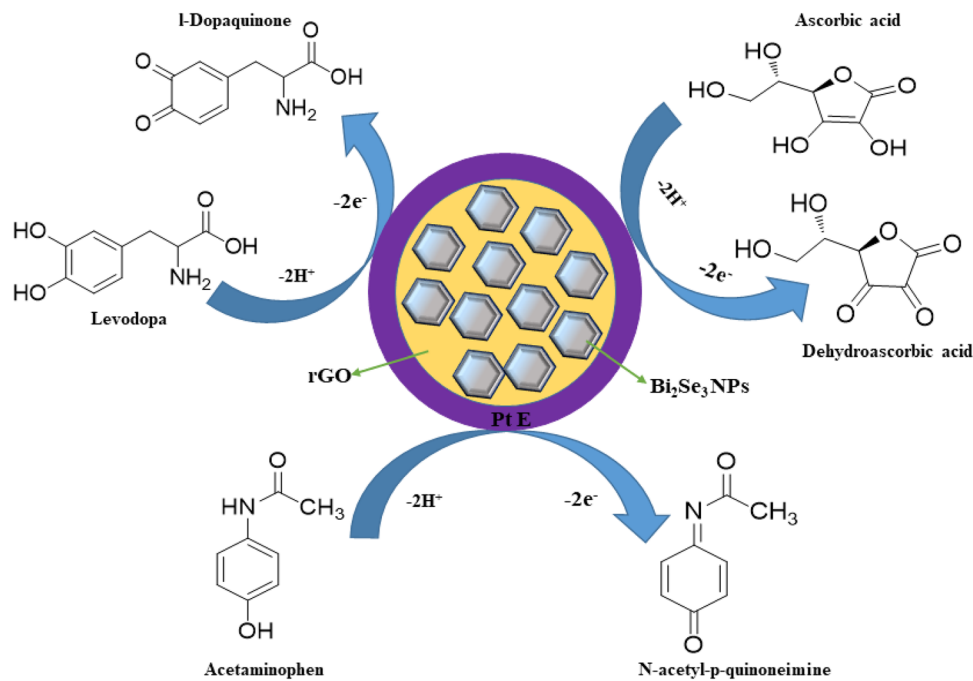


Fig. 7 Influence of accumulation **A** potential (V) **B** time on the oxidation peak current of 0.5 mM LD and ACT on Bi_2Se_3 NPs/rGO/Pt-E

However, the cathodic and anodic peak potentials shifted to both negative and positive sides. The Randles–Sevcik equation was used to determine the microscopic area of bare and modified Pt-Es [46]:

$$i_{pa} = 2.69 \times 10^5 AC_0 n^{3/2} D_R^{1/2} v^{1/2} \quad (3)$$

The peak current, electrode surface area, $\text{K}_3\text{Fe}(\text{CN})_6$ concentration, number of electrons transferred, diffusion coefficient, and scan rate are represented by I_p , A , C_0 , n , D_R , and v , respectively. From the slope of the $i_{pc}-v^{1/2}$ graph, the D_R was calculated as $6.7 \times 10^{-6} \text{ cm}^2 \text{ s}^{-1}$. The surface area of Bi_2Se_3 NPs/rGO/Pt-E was calculated as 0.752 cm^2 , which is six times higher than that of bare Pt-E.

Furthermore, the current potential responses were examined to assess the electrochemical performance of the Bi_2Se_3

NPs/rGO/Pt-E sensor for LD and ACT sensing in pharmaceuticals and biological samples. The microscopic areas of the electrodes are influenced by the peak responses of LD and ACT. In a phosphate buffer of pH 6.0 (10 mL) and scan rate of 10 mV/s, a comparison investigation was conducted on peak currents (i_{pa}) utilizing CV. Peak currents were proportional to the amount of electroactive surface area. The electrochemical responses of LD and ACT at +0.25 and +0.52 V (vs Ag/AgCl) representing curves a, b and c for bare Pt-E, rGO/Pt-E and Bi_2Se_3 NPs/rGO/Pt-E, respectively, as illustrated in Fig. 5C, D. Both compounds showed broad and weak intensity waves at +0.25 and +0.52 V due to the sluggish electron transport kinetics of the oxidation process at bare Pt-E. Modification of electrodes with rGO enhances the voltammetric signals (intensity anodic peaks) of LD and ACT at the same potentials.



The catalytic mechanism behind the detection of LD and ACT depends on the n-type semiconducting behaviour of Bi_2Se_3 NPs due to the charges on the selenium vacancies leading to the lattice defects and resulted as electron donors. The covalently bonded monolayers of five sets are in the order of Se-Bi-Se-Bi-Se, in which Se is assembled on either side, resulted as a bidentate ligand. During the electrochemical process, one electron trapping step occurs on the surface of Bi_2Se_3 at 0.41 V, converting Bi_2Se_3 NPs to $\text{Bi}_2\text{Se}_3^{\cdot-}$ species at -0.60 V, which is stimulated upon oxidation. When LD and ACT interact with radical anion ($\text{Bi}_2\text{Se}_3^{\cdot-}$), reduction occurs resulting in the conversion of $\text{Bi}_2\text{Se}_3^{\cdot-}$ to Bi_2Se_3 , followed by the oxidation of analytes. As a result, Bi_2Se_3 acts as an efficient electrocatalyst for the oxidation of LD and ACT, with the degree of oxidation proportional to the current generated. Considering a previous study by Savariraj et al., 2019 where Bi_2Se_3 was used as an electrocatalyst to fabricate the non-enzymatic glucose sensor, Bi_2Se_3 has been used as a mediator to enhance the electron transfer between the electrode and analytes in the electrochemical detection of LD and ACT with Bi_2Se_3 . [47].

For comparison, a study was performed on the LD and ACT response with Bi_2Se_3 NPs coated Pt-E, however, it is difficult to coated Bi_2Se_3 NPs alone due to low density and less adhesion property. The high loading of Bi_2Se_3 NPs and greater concentration of nafion on the surface of Pt-E shows no significant changes in the results as illustrated in Fig. 5C, D, where the peak currents achieved for both the compounds with rGO and pure Bi_2Se_3 NPs are almost in the same range. However, the electrochemical signaling of LD and ACT was greatly improved at Pt-E modified with rGO and Bi_2Se_3 NPs. The bar graph (inset Fig. 5C, D) exhibited relative current responses of three electrodes studied, demonstrating that the peak currents with Bi_2Se_3 NPs/rGO/Pt-E at $59.2 \mu\text{A}$ (LD) and $46.5 \mu\text{A}$ (ACT) were remarkably greater than that of currents obtained with bare Pt-E, rGO/Pt-E and Bi_2Se_3 /Pt-E at $3.1 \mu\text{A}$ (LD), $5.2 \mu\text{A}$ (ACT) and $6.2 \mu\text{A}$ (LD), $10.4 \mu\text{A}$ (ACT) and $7.5 \mu\text{A}$ (LD) and $8.3 \mu\text{A}$ (ACT), respectively.

Using Bi_2Se_3 NPs/rGO/Pt-E, cyclic voltammetry was used to investigate simultaneous electrochemical detection of LD and ACT in the presence of AA, as shown in Fig. 8A. A well-defined anodic peaks were observed at

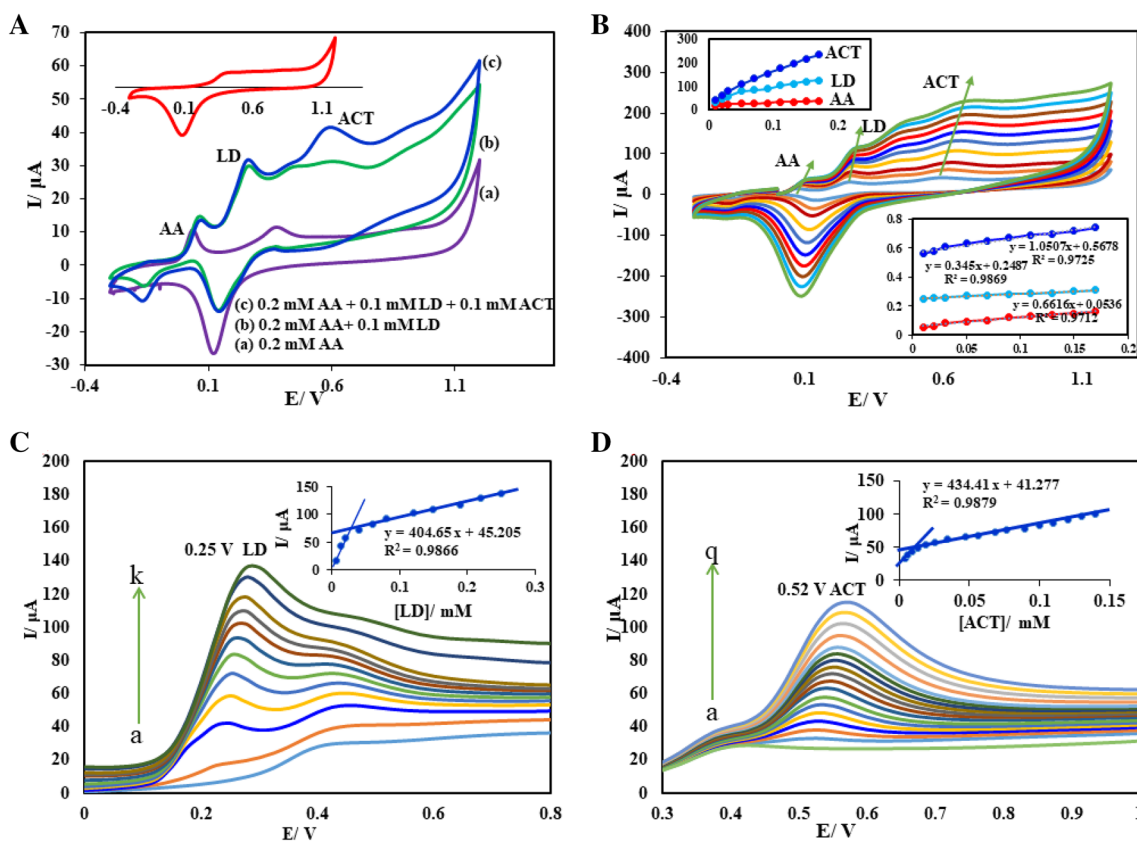


Fig. 8 A Cyclic voltammograms for simultaneous detection of three analytes on Bi_2Se_3 NPs/rGO/Pt-E a AA b AA+LD c AA+LD+ACT and in inset response of Bi_2Se_3 NPs/rGO/Pt-E without analytes B Cyclic voltammograms recorded at different scan rates at Bi_2Se_3 NPs/rGO/Pt-E and inset showing the plots of peak poten-

tials vs scan rate and peak currents vs scan rate C Typical DPVs of LD at studied concentration range in 0.1 M phosphate buffer (pH 6.0) and inset calibration plot of I_p vs [LD] D Typical DPVs of ACT at studied concentration range in 0.1 M phosphate buffer (pH 6.0) and inset calibration plot of I_p vs [ACT]



0.05 V for 0.2 mM AA (curve a), at 0.05 V for 0.2 mM AA + 0.25 V for 0.1 mM LD (curve b), at 0.05 V for 0.2 mM AA + 0.25 V for 0.1 mM LD + 0.57 V for 0.1 mM ACT (curve c). The AA, LD and ACT exhibited distinct anodic peaks at 0.05, 0.25 and 0.57 V with a peak to peak separation of 0.20 V (between AA and LD), 0.52 V (between AA and ACT), 0.32 (between LD and ACT) as shown in the inset showing the response of Bi₂Se₃ NPs/rGO/Pt-E in 0.1 M PBS. The anodic peaks resulted from Bi₂Se₃ NPs/rGO/Pt-E has greater separation efficiency for the concurrent sensing of LD and ACT in the sight of AA and further in any mixture. The efficient electrocatalytic effect of Bi₂Se₃ NPs/rGO/Pt-E was monitored by the oxidation of LD and ACT with sharp peaks, good selectivity, large peak separations and enhanced current responses, resulting in the amplification of electrochemical signaling of LD and ACT. The enhancement in both LD and ACT peak currents is due to the greater area of the layer on the surface of modified Pt-E and improvement in the electron transfer process.

To obtain the kinetic parameters, the effect of scan rates on the peak currents were studied with 0.2, 0.1 mM and 0.1 mM solutions of AA, LD and ACT on Bi₂Se₃ NPs/rGO/Pt-E using CV mode. Figure 8B shows the anodic peak currents for three compounds were linearly increases with an increase in the scan rate from 10 to 170 mV/s, indicating the oxidation process was adsorption controlled. Consequently, AA, LD, and ACT are first adsorbed and accumulated on the electrode surface and then followed by an electrochemical reduction reaction. The adsorbed quantities of analytes (AA, LD, and ACT) on the Pt-E surface was calculated using the following equation:

$$I_p = \frac{nFQv}{4RT} = \frac{n^2F^2AI^-T^v}{4RT} \quad (4)$$

The Faraday's constant is F (C mol⁻¹), Q (C) is the quantity of charge spent during the electro-oxidation reaction, and v (Vs⁻¹) is the scan rate. The area of the electrode is A (cm²), and the surface concentration of the electroactive AA, LD, and ACT is I^-_T (mol cm⁻²).

Integration of the peak area of modified Pt-Es, resulted in a straight line with a slope of 0.11 and 0.50 and 1.1 within the same scan range for AA, LD and ACT, respectively. From Eq. (4) the values of n and I^-_T were obtained and the results were 0.32, 1.6 and 3.1×10^{-6} , respectively. At an optimum scan rate of 50 mV/s, Bi₂Se₃ NPs/rGO/Pt-E showed 24.8, 79.8 and 108 μ A of the peak current, which was nearly tenfold compared to peak current measured at bare Pt-E (2.8, 8.4, and 11.7 μ A) for AA, LD and ACT indicate the fair catalytic activity of nanocomposite materials.

The effect of scan rate on the peak potentials was studied with the same concentration of AA, LD and ACT, and

the anodic peak potential shifted to a more positive side with an increase in the scan rate. The linear regression equations were constructed between the peak potentials and the scan rates (v) at the modified Pt-Es were shown in Fig. 8B.

$$I_{pa}(\mu A) = 0.6616v + 0.0536 \text{ (Vs}^{-1}\text{)} \text{ (} R^2 = 0.9712\text{)} \text{ AA} \quad (5)$$

$$I_{pa}(\mu A) = 0.345v + 0.2487 \text{ (Vs}^{-1}\text{)} \text{ (} R^2 = 0.9869\text{)} \text{ LD} \quad (6)$$

$$I_{pa}(\mu A) = 1.0507v + 0.5678 \text{ (Vs}^{-1}\text{)} \text{ (} R^2 = 0.9725\text{)} \text{ ACT} \quad (7)$$

From the regression equation, the electrochemical parameters, electron transfer co-efficient (α) 0.37 and 0.48 for both LD and ACT, and the electrode reaction standard rate constant (k_s) 1.73 and 2.17 s⁻¹ were calculated using Laviron's equation at the modified electrode.

$$E_{pa} = E^0 + \frac{RT}{(1 - \alpha)nF} \ln v \quad (8)$$

$$\log k_s = \alpha \log (1 - \alpha) + (1 - \alpha) \log \alpha - \log \frac{RT}{nFv} - \frac{(1 - \alpha)anF\Delta E_p}{2.3RT} \quad (9)$$

Quantification studies of LD and ACT with DPV

The DPV responses for various concentrations of LD and ACT at the modified electrode in 0.1 M phosphate buffer (pH 6.0) were measured individually under the best experimental conditions (pH 6.0, accumulation time: 100 s, accumulation potential: - 0.25 mV, pulse amplitude: 50 mV, voltage step: 2 mV, voltage step time: 0.4 s). The results revealed a linear relationship between the peak currents recorded and LD concentrations ranging from 0.006 to 0.25 mM, as shown in Fig. 8C. The peak current at a potential of +0.25 V (vs Ag/AgCl) increases sensitively with an increase in the concentration of LD. The linear regression equation for LD was obtained as $I_{pa}(\mu A) = 404.65C + 45.205$ ($R^2 = 0.9866$) with a limit of detection (LOD) and limit of quantification (LOQ) of 0.23 and 0.71 μ M, respectively, at the signal to noise ratio of 3. Similarly, a linear relationship between the peak currents and concentration ranging from 0.0045 to 0.14 mM of ACT was observed as shown in Fig. 8D. The peak current at a potential of +0.52 V (vs Ag/AgCl) increases gradually with an increase in the concentration of ACT. The calculated linear regression equation was noted as $I_{pa}(\mu A) = 434.41C + 41.277$ ($R^2 = 0.9879$) with a LOD and LOQ values of 0.17 μ M and 0.53 μ M respectively, at signal to noise ratio of 3. The split in the LD and ACT



calibration curves is most likely due to the creation of a sub-monolayer at low concentrations and a monolayer at high concentrations in the calibration plot.

The DPV studies were used to detect LD, ACT in the sight of AA concurrently. Three well-defined peaks were seen in Fig. 9A, showing that the Bi₂Se₃ NPs/rGO/Pt-E electrochemical sensor was an acceptable electrochemical sensor for concurrent sensing of two analytes. Peak currents for LD, ACT, and AA rose as concentration increased. The calibration curves were linear in some ranges when the peak potentials were constant (Fig. 9B). These findings suggest that Bi₂Se₃ NPs/rGO/Pt-E had adequate linear ranges and detection limits for simultaneously detecting LD and ACT in the presence of AA. The linear regression equations achieved for both LD and ACT are shown in (Fig. 9B).

$$I_{pa}(\mu A) = 477.54C + 21.286 \quad (R^2 = 0.991) \quad (10)$$

$$I_{pa}(\mu A) = 348.53C + 71.525 \quad (R^2 = 0.9914) \quad (11)$$

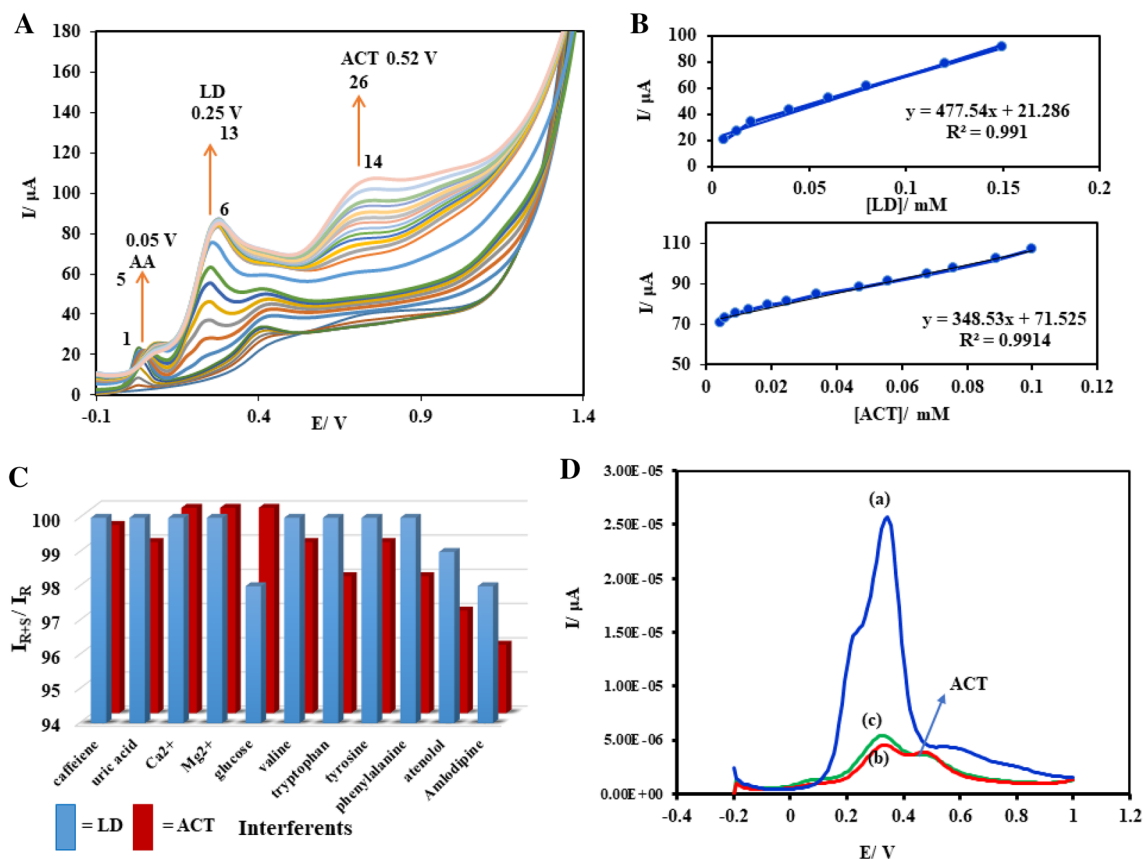


Fig. 9 A DPVs for simultaneous detection of three analytes on Bi₂Se₃ NPs/rGO/Pt-E for AA (1–5 additions), LD (6–13), ACT (14–26) B Calibration plots of I_p vs [LD] and I_p vs [ACT] for studied concentration ranges C Bar diagram showing the selectivity of Bi₂Se₃ NPs/

The analytical performance of the proposed electrode was summarized and compared with literature reports as tabulated in Table 2. The fabricated electrochemical sensor, Bi₂Se₃ NPs/rGO/Pt-E exhibited lower linear range and detection limits compared to the reported electrochemical sensors. Therefore, it could open a new venue for the simultaneous detection of LD and ACT in the presence of AA with ultra-sensitivity and high selectivity.

Validation of Bi₂Se₃ NPs/rGO/Pt-E

The fabricated electrochemical sensor was verified by measuring the parameters such as robustness, precision, accuracy, recovery, and selectivity. Five replicate measurements on 0.1 mM LD and ACT assay were done on the first day (intra-day) and after 5 days (inter-day) to determine the accuracy. The standard addition method was used to examine recovery and results were showed in Table 3. To test the sensor's stability, it was submerged in PBS (pH 6.0) containing LD and ACT for 5 days and the voltammograms were recorded. The results were compared with the voltammograms of the

rGO/Pt-E for LD and ACT in the presence of different interferents and their I_{R+S}/I_R values D DPVs for LD injection (a) and ACT tablet real samples (b, c)

Table 2 Comparison of various reported electrochemical sensors with that of present electrochemical sensor for the simultaneous detection of LD and ACT

Analyte	Electrode	Modifier	LDR	LOD	References
LD	Carbon paste	Hemoglobin electrostatic immobilized on WO ₃ nanoparticles	60–1070 μM	0.25 μM	[48]
LD	Graphite–polyurethane	Oxovanadium-salen	10–300 μM	0.8 μM	[49]
LD	Glassy carbon	Cyclodextrine doped poly (2,5diamino-benzene sulfonic acid)	7–200 μM	0.418 μM	[50]
ACT	Glassy carbon disk	Tetraruthenated cobalt(II) porphyrin intercalated into a smectite clay	1–50 μM	0.1 μM	[51]
ACT	Glassy carbon electrode	Polymer and multi-walled carbon nanotubes	5.0–1000.0 μM	3.5 μM	[52]
ACT	Glassy carbon	Carbon-coated nickel magnetic nanoparticles	30–700 μM	2.3 μM	[53]
LD	carbon paste	Graphene and ethyl	0.2–0.4 mM	0.07 μM	[2]
ACT		2-(4-ferrocenyl-[1,2,3]triazol-1-yl) acetate	1.0–0.15 mM	0.5 μM	
TYR			5.0–0.18 mM	2.0 μM	
LD	Glassy carbon	Luteolin/(fMWCNT/GCE)	0.7–100.0 μM	0.25 μM	[54]
ACT			1.0–90.0 μM	0.52 μM	
TYR			0.5–70.0 μM,	0.12 μM	
LD	Glassy carbon	Nickel	0.1–100 μM	0.076 μM	[55]
ACT		Hydroxide nanoparticles/multi-walled carbon nanotubes	0.06–26 μM	0.017 μM	
LD	carbon paste electrode	TiO ₂ hollow sphere/multi-walled	0.4–450 μM	0.105 μM	[18]
ACT		carbon nanotube/poly-aspartic acid composite	0.1–300 μM	0.07 μM	
LD	Pt electrode	Bi ₂ Se ₃ NPs/rGO	0.006–0.25 mM	0.23 μM	Present work
ACT			0.0045–0.14 mM	0.17 μM	

Table 3 Analytical parameters [accuracy, precision and recovery ($n=5$)] obtained for LD and ACT at Bi₂Se₃ NPs/rGO/Pt-E

Method	Analyte	Concentration added (mM)	Concentration found (mM)	Bias ^a	Recovery (%)	Precision RSD ^b ($n=5$)
DPV	LD	Intraday (0.1)	0.098	– 0.902	98	0.67
		Inter day (0.1)	0.092	– 0.908	92	0.87
	ACT	Intraday (0.1)	0.096	– 0.904	96	1.31
		Inter day (0.1)	0.090	– 0.910	90	0.92

^aBias = (found-added/added)^bRelative standard deviation for five individual determinations

same sensor obtained after every 5 days. The obtained data revealed that the peak currents decreased slightly, indicating that the developed electrochemical sensor possessed long-term stability. In the presence of excipients including uric acid, caffeine, calcium (II), magnesium (II), tryptophan, valine, tyrosine, glucose, atenolol, phenylalanine, and Amlodipine, the capacity of the optimized technique to detect LD and ACT selectively was investigated. The degree of substantial interference with LD and ACT was evaluated using the current ratio method. The peak currents obtained from LD and ACT were measured alone (I_R) in 0.5 mM of excipient substance (I_{R+S}). The current ratios (I_{R+S}/I_R) of LD and ACT were in the range of 0.92 ± 0.05 to 1.01 ± 0.03 for above mentioned co-existing interferences, respectively (Fig. 9C). The current ratios were unchanged in the presence of interferences, indicating that the fabricated electrochemical sensor possessed an excellent selectivity towards the analytes. Variations in some of the key factors, such

as preconcentration, time, pH, and potential, were used to assess the robustness. The obtained findings demonstrated the manufactured electrochemical sensor's dependability in the analysis of LD and ACT. Within the analyzed range of operational parameter adjustments, the mean % recoveries of five replicate measurements were not significantly altered, indicating that the Bi₂Se₃ NPs/rGO/Pt-E is a reliable electrochemical sensor.

Analytical applications

By analyzing pharmaceuticals and synthetic urine samples, the analytical applications of the constructed sensor (Bi₂Se₃ NPs/rGO/Pt-E) were investigated to detect LD and ACT. The standard addition method was used to analyze the real and urine samples at Bi₂Se₃ NPs/rGO/Pt-E to avoid the matrix effect. The voltammetric responses of urine and actual samples spiked with known concentrations of LD and



Table 4 Detection of the LD and ACT in synthetic urine and real pharmaceutical samples

Sample	LD added (μM)	LD found (μM)	Recovery (%)	RSD ^e (%)	ACT added (μM)	ACT found (μM)	Recovery (%)	RSD ^e (%)
^a U. S 1	10.0	9.93 (± 0.03)	99.3	0.78	10.0	10.22 (± 0.03)	102.2	0.92
U. S 2	15.0	15.18 (± 0.02)	101.2	0.91	20.0	19.16 (± 0.03)	98.0	1.12
U. S 3	25.0	24.8 (± 0.02)	99.2	0.88	30.0	29.84 (± 0.01)	99.5	0.95
^b Injection sample	10.0	9.12 (± 0.01)	91.2	1.3	–	–	–	–
^c Ancogen Tablet	–	–	–	–	15	14.61 (± 0.02)	97.4	1.2
^d SOMA Tablet	–	–	–	–	15	14.37 (± 0.01)	95.8	0.92

^aU.S=Synthetic urine samples

^bTaiwan Biotech CO., LTD, Taiwan

^cHua Shin Chemical Pharmaceutical works CO., LT, Taiwan

^dStandard Chem & Pharm CO., LTD, Taiwan

^eRelative standard deviation for five individual determination

ACT were recorded after they were diluted [4 times with 0.1 M PBS (pH 6.0) without any pretreatment]. The results showed that the Bi_2Se_3 NPs/rGO/Pt-E sensor is reliable, it could be successfully applied to the detection of LD and ACT in real pharmaceutical and urine samples (Table 4 and Fig. 9D).

Conclusions

The novel fabricated electrochemical sensor, Bi_2Se_3 NPs/rGO/Pt-E has exceptional properties such as excellent adsorptive properties, electrocatalytic properties, and high specific surface area. To our knowledge, this is the first time that Bi_2Se_3 NPs/rGO/Pt-E were used to selectively recognize and sensitively determine LD and ACT in the presence of AA. For the simultaneous detection of LD and ACT, the electrochemical characteristics of all three electrodes, bare Pt-E, rGO/Pt-E, and Bi_2Se_3 NPs/rGO/Pt-E, have been studied. Interestingly, it was noticed that Bi_2Se_3 NPs/rGO/Pt-E exhibited high selectivity and ultra-sensitivity towards LD and ACT. In comparison to previous methods published in the literature, the suggested method is very reliable and sensitive in reaching ultra-low detection limits, very good reproducibility, wide linear dynamic range, and repeatability. The proposed strategy is expected to be extremely beneficial to both the pharmaceutical industries and the clinical sector.

Acknowledgements We are grateful for the financial support of the Ministry of Science and Technology, Taiwan (MOST 104-2113-M-007-008-MY3 and MOST 104-2923-M-007-002-MY3) and the National Tsing Hua University for this work.

Author contributions The manuscript was written by G.G and AB through the contributions of all authors. G.G, A.B, and S.K. conceived ideas and G.G, A.B carried out the experiments and interpreted

the results. YCL and MR supervised the study. All authors read and approved the final manuscript.

Declarations

Conflict of interest The authors declare no conflict of interests.

References

1. Castro Caldas, A., Teodoro, T., Ferreira, J.J.: The launch of opi-capone for Parkinson's disease: negatives versus positives. *Expert Opin. Drug Saf.* **17**, 331–337 (2018)
2. Movlaee, K., Beitollahi, H., Ganjali, M.R., Norouzi, P.: Electrochemical platform for simultaneous determination of levodopa, acetaminophen and tyrosine using a graphene and ferrocene modified carbon paste electrode. *Microchim. Acta.* **184**, 3281–3289 (2017)
3. César, Id.C., Byrro, R.M.D., de Santana e Silva Cardoso, F.F., Mundim, I.M., de Souza Teixeira, L., Pontes da Silva, E., Gomes, S.A., Bonfim, R.R., Pianetti, G.A.: Simultaneous quantitation of levodopa and 3-O-methyldopa in human plasma by HPLC–ESI-MS/MS: Application for a pharmacokinetic study with a levodopa/benserazide formulation. *J. Pharm. Biomed. Anal.* **56**, 1094–1100 (2011)
4. Yue, H.Y., Zhang, H., Huang, S., Lin, X.Y., Gao, X., Chang, J., Yao, L.H., Jun Guo, Er.: Synthesis of ZnO nanowire arrays/3D graphene foam and application for determination of levodopa in the presence of uric acid. *Biosens Bioelectron.* **89**, 592–597 (2017)
5. Pistonesi, M., Centurión, M.E., Band, B.S.F., Damiani, P.C., Olivieri, A.C.: Simultaneous determination of levodopa and benserazide by stopped-flow injection analysis and three-way multivariate calibration of kinetic-spectrophotometric data. *J. Pharm. Biomed. Anal.* **36**, 541–547 (2014)
6. Hansson, C., Agrup, G., Rorsman, H., Rosengren, A.M., Rosengren, E., Edholm, L.E.: Analysis of cysteinyl-dopas, dopa, dopamine, noradrenaline and adrenaline in serum and urine using high-performance liquid chromatography and electrochemical detection. *J. Chromatogr. B Biomed. Appl.* **162**, 7–22 (1979)

7. He, W.-W., Zhou, X.-W., Lu, J.-Q.: Simultaneous determination of benserazide and levodopa by capillary electrophoresis–chemiluminescence using an improved interface. *J. Chromatogr. A*. **1131**, 289–292 (2006)
8. Soh, C.S., Raveendran, P.: Multi-resolution analysis of near infrared spectroscopic data for calibration and prediction of active substances in phosphate buffer solution, pp. 415–418. Springer, Berlin Heidelberg (2007)
9. Vilchez, J., Blanc, R., Avidad, R., Navalón, A.: Spectrofluorimetric determination of paracetamol in pharmaceuticals and biological fluids. *J. Pharm. Biomed. Anal.* **13**, 1119–1125 (1995)
10. Nebot, C., Gibb, S.W., Boyd, K.G.: Quantification of human pharmaceuticals in water samples by high performance liquid chromatography–tandem mass spectrometry. *Anal. Chim. Acta*. **598**, 87–94 (2007)
11. Săndulescu, R., Mirel, S., Oprean, R.: The development of spectrophotometric and electroanalytical methods for ascorbic acid and acetaminophen and their applications in the analysis of effervescent dosage forms. *J. Pharm. Biomed. Anal.* **23**, 77–87 (2000)
12. Perez-Ruiz, T., Martinez-Lozano, C., Tomas, V., Galera, R.: Migration behaviour and separation of acetaminophen and p-aminophenol in capillary zone electrophoresis: analysis of drugs based on acetaminophen. *J. Pharm. Biomed. Anal.* **38**, 87–93 (2005)
13. Kunene, K., Weber, M., Sabela, M., Voiry, D., Kanchi, S., Bisetty, K., Mikhael, B.: Highly-efficient electrochemical label-free immunosensor for the detection of ochratoxin A in coffee samples. *Sens. Actuators B Chem.* **305**, 127438 (2020)
14. Rezaei, B., Shams-Ghahfarokhi, L., Havakeshian, E., Ensafi, A.A.: An electrochemical biosensor based on nanoporous stainless steel modified by gold and palladium nanoparticles for simultaneous determination of levodopa and uric acid. *Talanta* **158**, 42–50 (2016)
15. Fouladgar, M., Karimi-Maleh, H., Gupta, V.K.: Highly sensitive voltammetric sensor based on NiO nanoparticle room temperature ionic liquid modified carbon paste electrode for levodopa analysis. *J. Mol. Liq.* **208**, 78–83 (2015)
16. Xu, Y., Lei, W., Su, J., Hu, J., Yu, X., Zhou, T., Yang, Y., Mandler, D., Hao, Q.: A high-performance electrochemical sensor based on g-C₃N₄-E-PEDOT for the determination of acetaminophen. *Electrochim. Acta*. **259**, 994–1003 (2018)
17. Yang, C., Zhu, S., Ma, J., Song, J., Ran, P., Fu, Y.: Highly sensitive electrochemical sensing platform for the detection of L-dopa based on electropolymerizing glutathione disulfide and multi-walled carbon nanotube-modified electrodes. *S. Afr. J. Chem.* **71**, 182–187 (2018)
18. Babaei, A., Sohrabi, M.: Selective simultaneous determination of levodopa and acetaminophen in the presence of ascorbic acid using a novel TiO₂ hollow sphere/multi-walled carbon nanotube/poly-aspartic acid composite modified carbon paste electrode. *Anal. Methods*. **8**, 1135–1144 (2016)
19. Zhang, Z., Fu, X., Li, K., Liu, R., Peng, D., He, L., Wang, M., Zhang, H., Zhou, L.: One-step fabrication of electrochemical biosensor based on DNA-modified three-dimensional reduced graphene oxide and chitosan nanocomposite for highly sensitive detection of Hg(II). *Sens. Actuators B Chem.* **225**, 453–462 (2016)
20. Venkatesh, K., Rajakumaran, R., Chen, S.-M., Karuppiyah, C., Yang, C.-C., Ramaraj, S.K., Ali, M.A., Al-Hemaid, F.M.A., El-Shikh, M.S., Almunqedhi, B.M.A.: A novel hybrid construction of MnMoO₄ nanorods anchored graphene nanosheets; an efficient electrocatalyst for the picomolar detection of ecological pollutant ornidazole in water and urine samples. *Chemosphere* **273**, 129665 (2021)
21. Zhu, C., Yang, G., Li, H., Du, D., Lin, Y.: Electrochemical sensors and biosensors based on nanomaterials and nanostructures. *Anal. Chem.* **87**, 230–249 (2015)
22. Serrano, N., Alberich, A., Díaz-Cruz, J., Ariño, C., Esteban, M.: Coating methods, modifiers and applications of bismuth screen-printed electrodes. *Trends Anal. Chem.* **46**, 15–29 (2013)
23. Wang, J., Lu, J., Hocevar, S.B., Farias, P.A.M., Ogorevc, B.: Bismuth-coated carbon electrodes for anodic stripping voltammetry. *Anal. Chem.* **72**, 3218–3222 (2000)
24. Lezi, N., Economou, A., Dimovasilis, P.A., Trikalitis, P.N., Prodromidis, M.I.: Disposable screen-printed sensors modified with bismuth precursor compounds for the rapid voltammetric screening of trace Pb(II) and Cd(II). *Anal. Chim. Acta*. **728**, 1–8 (2012)
25. Sopha, H., Baldrianová, L., Tesařová, E., Grncienė, G., Weidlich, T., Švancara, I., Hočevar, B.: A new type of bismuth electrode for electrochemical stripping analysis based on the ammonium tetrafluorobismuthate bulk-modified carbon paste. *Electroanalysis* **22**, 1489–1493 (2010)
26. Dimovasilis, P.A., Prodromidis, M.I.: Bismuth-dispersed xerogel-based composite films for trace Pb(II) and Cd(II) voltammetric determination. *Anal. Chim. Acta*. **769**, 49–55 (2013)
27. María-Hormigos, R., Gismera, M.J., Procopio, J.R., Sevilla, M.T.: Disposable screen-printed electrode modified with bismuth–PSS composites as high sensitive sensor for cadmium and lead determination. *J. Electroanal. Chem.* **767**, 114–122 (2016)
28. Rimán, D., Avgeropoulos, A., Hrbac, J., Prodromidis, M.I.: Sparked-bismuth oxide screen-printed electrodes for the determination of riboflavin in the sub-nanomolar range in non-deoxygenated solutions. *Electrochim. Acta*. **165**, 410–415 (2015)
29. de Lima, C.A., Spinelli, A.: Electrochemical behavior of progesterone at an ex situ bismuth film electrode. *Electrochim. Acta*. **107**, 542–548 (2013)
30. de Figueiredo-Filho, L.C.S., dos Santos, V.B., Janegitz, B.C., Guerreiro, T.B., Fatibello-Filho, O., Faria, R.C., Humberto, L., Junior, M.: Differential pulse voltammetric determination of paraquat using a bismuth-film electrode. *Electroanalysis* **22**, 1260–1266 (2010)
31. Sopha, H., Hocevar, S.B., Pihlar, B., Ogorevc, B.: Bismuth film electrode for stripping voltammetric measurement of sildenafil citrate. *Electrochim. Acta*. **60**, 274–277 (2012)
32. Tseliou, F., Avgeropoulos, A., Falaras, P., Prodromidis, M.I.: Low dimensional Bi₂Te₃-graphene oxide hybrid film-modified electrodes for ultra-sensitive stripping voltammetric detection of Pb(II) and Cd(II). *Electrochim. Acta*. **231**, 230–237 (2017)
33. Hummers, W.S., Offeman, R.E.: Preparation of graphitic oxide. *J. Am. Chem. Soc.* **80**, 1339–1339 (1958)
34. Gorle, G., Bathinapatla, A., Chen, Y.-Z., Ling, Y.-C.: Near infrared light activatable PEI-wrapped bismuth selenide nanocomposites for photothermal/photodynamic therapy induced bacterial inactivation and dye degradation. *RSC Adv.* **8**, 19827–19834 (2018)
35. Deroco, P.B., Vicentini, F.C., Oliveira, G.G., Rocha-Filho, R.C., Fatibello-Filho, O.: Square-wave voltammetric determination of hydroxychloroquine in pharmaceutical and synthetic urine samples using a cathodically pretreated boron-doped diamond electrode. *J. Electroanal. Chem.* **719**, 19–23 (2014)
36. Hennighausen, Z., Lane, C., Buda, I.G., Mathur, V.K., Bansil, A., Kar, S.: Evidence of a purely electronic two-dimensional lattice at the interface of TMD/Bi₂Se₃ heterostructures. *Nanoscale* **11**, 15929–15938 (2019)
37. Ota, J.R., Roy, P., Srivastava, S.K., Popovitz-Biro, R., Tenne, R.: A simple hydrothermal method for the growth of Bi₂Se₃ nanorods. *Nanotechnology* **17**, 1700–1705 (2006)
38. Xiao, C., Yang, J., Zhu, W., Peng, J., Zhang, J.: Electrodeposition and characterization of Bi₂Se₃ thin films by electrochemical



- atomic layer epitaxy (ECALE). *Electrochim. Acta.* **54**, 6821–6826 (2009)
39. Singh, P., Kim, Y.J., Wang, C., Mathiyalagan, R., Yang, D.C.: The development of a green approach for the biosynthesis of silver and gold nanoparticles by using *Panax ginseng* root extract, and their biological applications. *Artif. Cells Nanomed. Biotechnol.* **44**, 1150–1157 (2016)
40. Dun, C., Hewitt, C.A., Huang, H., Xu, J., Montgomery, D.S., Nie, W., Jiang, Q., Carroll, D.L.: Layered Bi₂Se₃ nanoplate/polyvinylidene fluoride composite based n-type thermoelectric fabrics. *ACS Appl. Mater. Interfaces.* **7**, 7054–7059 (2015)
41. Liu, M., Spanos, P.D., Yu, S.-H.: Synthesis of ultrathin Bi₂Se₃ nanosheets/graphene nanocomposite with defects/vacancies-dependent transient photocurrent performance. *Nano Energy* **64**, 103877 (2019)
42. Zhuang, A., Zhao, Y., Liu, X., Xu, M., Wang, Y., Jeong, U., Wang, X., Zeng, J.: Controlling the lateral and vertical dimensions of Bi₂Se₃ nanoplates via seeded growth. *Nano Res.* **8**, 246–256 (2015)
43. Chaiyakun, S., Witit-anun, N., Nuntawong, N., Chindaudom, P., Oaew, S., Kedkeaw, C., Limsuwande, P.: Preparation and characterization of graphene oxide nanosheets. *Procedia Eng.* **32**(759), 764 (2012)
44. Yang, D., Velamakanni, A., Bozoklu, G., Park, S., Stoller, M., Piner, R.D., Stankovich, S., Jung, I., Field, D.A., Ventrice Jr, C.A., Ruoffa, R.S.: Chemical analysis of graphene oxide films after heat and chemical treatments by X-ray photoelectron and Micro-Raman spectroscopy. *Carbon* **47**, 145–152 (2009)
45. Sun, Z., Liufu, S., Chen, L.: Synthesis and characterization of nanostructured bismuth selenide thin films. *Dalton Trans.* **39**, 10883–10887 (2010)
46. Suvardhan, K., Heba, A.K.: Electrochemical biosensor for the detection of amygdalin in apple seeds with a hybrid of f-MWCNTs/CoFe₂O₄ nanocomposite. *Curr. Anal. Chem.* **16**, 660–668 (2020)
47. Savariraj, A.D., Vinoth, V., Mangalaraja, R.V., Arun, T., Contreras, D., Akbari-Fakhrabadi, A., Valdés, H., Banat, F.: Microwave-assisted synthesis of localized surface plasmon resonance enhanced bismuth selenide (Bi₂Se₃) layers for non-enzymatic glucose sensing. *J. Electroanal. Chem.* **856**, 113629 (2020)
48. Ghodsi, J., Rafati, A.A., Shoja, Y.: First report on hemoglobin electrostatic immobilization on WO₃ nanoparticles: application in the simultaneous determination of levodopa, uric acid, and folic acid. *Anal. Bioanal. Chem.* **408**, 3899–3909 (2016)
49. Teixeira, M.F.S., Marcolino-Júnior, L.H., Fatibello-Filho, O., Dockal, E.R., Bergamini, M.F.: An electrochemical sensor for l-dopa based on oxovanadium-salen thin film electrode applied flow injection system. *Sens. Actuators B Chem.* **122**, 549–555 (2007)
50. Aslanoglu, M., Kutluay, A., Goktas, S., Karabulut, S.: Voltammetric behaviour of levodopa and its quantification in pharmaceuticals using a β -cyclodextrine doped poly (2,5-diaminobenzenesulfonic acid) modified electrode. *J. Chem. Sci.* **121**, 209–215 (2009)
51. Kemmegne-Mbouguen, J.C., Toma, H.E., Araki, K., Constantino, V.R.L., Ngameni, E., Angnes, L.: Simultaneous determination of acetaminophen and tyrosine using a glassy carbon electrode modified with a tetraruthenated cobalt(II) porphyrin intercalated into a smectite clay. *Microchim. Acta.* **183**, 3243–3253 (2016)
52. Liu, R., Zeng, X., Liu, J., Luo, J., Zheng, Y., Liu, X.: A glassy carbon electrode modified with an amphiphilic, electroactive and photosensitive polymer and with multi-walled carbon nanotubes for simultaneous determination of dopamine and paracetamol. *Microchim. Acta.* **183**, 1543–1551 (2016)
53. Wang, S.-F., Xie, F., Hu, R.-F.: Carbon-coated nickel magnetic nanoparticles modified electrodes as a sensor for determination of acetaminophen. *Sens. Actuators B Chem.* **123**, 495–500 (2007)
54. Baghayeri, M., Namadchian, M.: Fabrication of a nanostructured luteolin biosensor for simultaneous determination of levodopa in the presence of acetaminophen and tyramine: application to the analysis of some real samples. *Electrochim. Acta.* **108**, 22–31 (2013)
55. Babaei, A., Sohrabi, M., Taheri, A.R.: Highly sensitive simultaneous determination of l-dopa and paracetamol using a glassy carbon electrode modified with a composite of nickel hydroxide nanoparticles/multi-walled carbon nanotubes. *J. Electroanal. Chem.* **698**, 45–51 (2013)

Publisher's Note Springer Nature remains neutral with regard to jurisdictional claims in published maps and institutional affiliations.